18th International Conference on Information Fusion
Washington, DC - July 6-9, 2015

Challenges of Multi-Target Tracking for Space Situational Awareness

Brandon A. Jones
Daniel S. Bryant
Department of Aerospace Engineering Sciences
University of Colorado Boulder
Boulder, Colorado 80309
Email: Brandon.Jones@colorado.edu
Daniel.Bryant@colorado.edu

Ba-Tuong Vo
Ba-Ngu Vo
Department of Electrical and Computer Engineering
Curtin University
Perth, Australia
Email: ba-tuong.vo@curtin.edu.au
ba-ngu.vo@curtin.edu.au

***Abstract*—The tracking of space objects poses unique challenges when compared to traditional applications. Direct application of standard multi-target tracking models fails to yield accurate results for the case of space objects. For example, dynamic models for traditional applications require simple, often linear, discrete-time models. This is not the case for space objects where motion is nonlinear and computation cost is too prohibitive for current Monte Carlo filters. This paper describes the multi-target tracking problem for space objects and summarizes system requirements for space situational awareness. Traditional multi-target filter models are compared to corresponding methods for space object tracking in the context of tracking performance via the δ-Generalized Labeled Multi-Bernoulli (δ-GLMB) filter. Using these tests, key research challenges for space situational awareness are discussed.**

I. Introduction

This paper discusses the needs for multi-target tracking in the context of space situational awareness (SSA). Recent research in the astrodynamics community suggests that improved methods of multi-target tracking for tracking space object provide a potential means to reduce uncorrelated tracks (UCTs) and improve orbit state estimates [1]–[5]. A common element among all of these papers is that customization of each technique is required for astrodynamics applications. This paper outlines some of the challenges in tracking space objects that, in some cases, are deemed of less importance for many traditional multi-target tracking problems.

Definitions of the term space situational awareness vary, but it typically refers to maintaining knowledge of the space environment to aid in risk assessment and to ensure sustainability. Traditionally, the tracking of thousands of objects via ground-based sensors, e.g., radar and telescopes, allowed for the estimation and prediction of a space object catalog. Objects in such a catalog, typically dubbed resident space objects (RSOs), include active spacecraft, decommissioned payloads, and debris from fragmentation events (e.g., insulation delamination events, collisions, explosions, etc.). Events in the late 2000s forced the SSA community to reevaluate methods employed since the 1960s. This culminated in an assessment of the U.S. Air Force's existing astrodynamics standards and practices [6]. Included among the recommendations were: (i) the development of improved data association methods, (ii) improve estimation algorithms to better account for nonlinearities and produce improved uncertainty estimates, and (iii) be able to handle a possible increase in catalog size to more than 100,000 RSOs. This paper discusses some of the challenges in multi-target tracking associated with these recommendations.

The paper is outlined as follows. The next section discusses the difficulties of tracking multiple RSOs, which includes an outline of some of the issues resulting from astrodynamics-based elements. Section III outlines the multi-target filter employed here to illustrate some of the challenges, along with some models commonly employed for traditional applications and their astrodynamics-based equivalent. Section IV demonstrates some of the difficulties of tracking space objects using the common astrodynamics models. Finally, conclusions and recommendations for future research are discussed.

II. Space Situational Awareness Requirements

A. General Overview

SSA requires knowledge of the current and predicted states of the RSO population. To maintain such information, the Joint Space Operations Center (JSpOC) collects and processes 400,000 observations per day to update the estimated states for over 20,000 objects [6]. Many of the tracked objects are persistent, i.e., there is a priori knowledge of their existence, however, new objects appear in the Space Surveillance Network's (SSN) surveillance regions due to launches of new space vehicles and fragmentation events. As demonstrated by the collision between Iridium 33 and Kosmos-2251, large-scale breakup events are an eventuality. Additionally, development of new observation capabilities will yield an increase in the number of trackable objects. Detecting and classifying these new objects is one of the goals of SSA, which requires multi-target tracking on a large scale.

Other goals of SSA includes conjunction assessment (CA) and object characterization. CA includes the prediction of potential collisions between space objects to provide timely and actionable information to operators. Taking a brute force approach, this requires the propagation of the entire space object catalog through time and the estimation of collision

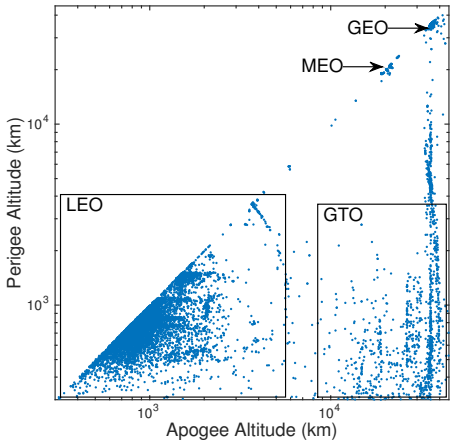

Fig. 1. Distribution of space objects as a function of altitude

probabilities for all possible object pairings. Several filters have been presented that alleviate the inherent computational load of such an approach (e.g., see [7]). Additionally, current approaches to CA only consider RSOs in a given object catalog. Alternatively, engineering tools (e.g., NASA's ORDEM and ESA's MASTER) provide an assessment of spacecraft risk based on debris flux that includes knowledge of trackable (>10 cm) and un-trackable objects, but no top-down tools currently exist that treat all knowledge of the debris population as a whole. Object characterization includes the determination of an object's shape, attitude, and other pertinent properties [6]. Shape and attitude information is required to improve state prediction. Such knowledge of an object also provides insight about predicted radar and optical observations. Approaches to RSO characterization include [8] and [9], but remain an active area of research.

Fig. 1 presents the distribution of the trackable objects in Earth orbit on February 27, 2013[1] as a function of their apogee and perigee altitudes. Objects along the diagonal are in a circular orbit, which includes those in Medium Earth Orbit (MEO) and Geosynchronous Orbit (GEO) satellites. Objects in Geosynchronous Transfer Orbit (GTO) exhibit large variations in their orbit state and are difficult to acquire. Finally, most objects are in Low Earth Orbit (LEO). Such objects have an orbit period of approximately 90 minutes, and, due to sparsity in sensors for tracking, can orbit up to hundreds of times between observation sets. The propagation of uncertainty for such cases makes measurement-to-track correlation more difficult. Even though MEO and GEO objects tend to be easier to track, their importance to commerce (e.g., satellite navigation or telecommunications) motivates improved state estimation accuracy to ensure viability and safety.

[1]Two-line element sets provided by CelesTrak (http://www.celestrak.com) and accessed on March 5, 2013.

B. Modeling RSOs

Modeling the dynamics of a space object requires a continuous time model based on the differential equation

$$\ddot{\boldsymbol{r}} = -\frac{\mu}{\|\boldsymbol{r}\|}\boldsymbol{r} + \boldsymbol{a}_p \tag{1}$$

with position vector $\boldsymbol{r}$, gravitation parameter μ, and perturbing accelerations $\boldsymbol{a}_p$. The complexity in modeling the translation dynamics of a spacecraft is rooted in the modeling of these perturbing accelerations. These perturbations can include, but are not limited to: the aspherical mass distribution in the primary body, third-body perturbations, solar radiation pressure (SRP), atmospheric drag, attitude-dependent effects, maneuvers, and many others. The magnitude of each varies with orbit regime. For example, atmospheric drag is the dominant non-gravitational perturbation when below 900 km in altitude. However, at higher altitudes where the effects of atmospheric drag begin to diminish, the effects of SRP and third-body perturbations become more pronounced. Both drag and SRP vary with space object attitude, making the modeling of such forces more difficult.

The need for attitude and shape estimation is made most evident by the dynamics observed for High-Area-to-Mass Ratio (HAMR) objects. Such objects exhibit variations in orbit declination near GEO that are not feasible given only gravitational forces [10], and predicting their trajectory requires knowledge of target-specific properties. The presence of such objects motivates continued refinement of force and torque models for RSOs, which directly impacts multi-target tracking.

One element that creates difficulty for tracking space objects is the detection of a maneuver. Maneuver estimation is further made difficult by the inability to distinguish it from mismodeled dynamics. Current research attempts to estimate possible maneuvers based on optimal control theory [11], but this has not yet been integrated with any multi-target filter in the literature. While methods exist for maneuver detection within the context of a multi-target tracker (e.g., see description in [12]), limited knowledge on the dynamics environment adds challenges to such a process [11].

Coupled with the prediction of the translation state of an RSO is the propagation of its state Probability Density Function (PDF). Traditionally, such propagation uses a state transition matrix to map a covariance matrix in time. As implied by (1), propagation of a prior Gaussian state PDF will yield non-zero cumulants over time [13]. Improved representations of a propagated state PDF are required for CA, maneuver detection, sensor tasking, and other important elements related to SSA. Details on possible methods are described later in the context of multi-target filtering.

C. Data Sources and Limitations

The SSN consists of both electro-optical and radio-frequency sensors, where phased array radars contribute the bulk of radar observations [14]. Radars are typically used for observing objects in LEO and can collect a combination of range, range-rate, azimuth and elevation observations. Optical

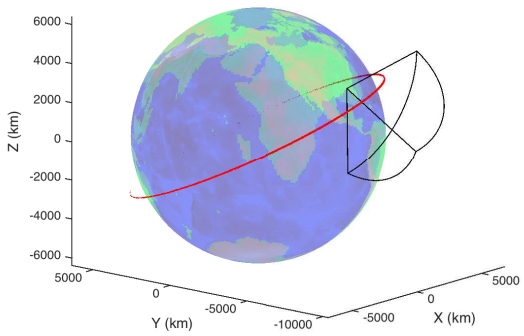

Fig. 2. Non-Gaussian uncertainty after ∼32 hours of propagation for a low-Earth orbiter. Red dots are samples from the state PDF and black lines indicate a sample field of view for a phased-array radar.

sensors measure right ascension and declination angles and are typically used to collect observations of objects in MEO and GEO. To estimate such angular quantities, detection of an RSO is compared to background stars [15]. Locations, limitations, and calibration values for many of the available SSN sensors are tabulated in [14], [16].

SSN sensors can collect observations at relatively high frequencies that are sufficient for orbit determination [16], however, long periods of time can pass between observations of a single object. Observations are typically collected in either long or short arcs (the former preferred over the latter) and it is the time gaps between these arcs that pose problems for tracking RSOs. Long observation gaps translate into high integration times and non-Gaussian state PDFs. Fig. 2 illustrates this point. Using the test case presented in [17] with initial position standard deviations on the order of 20 km, 100,000 samples are propagated forward in time, yielding a non-Gaussian state PDF after 32.38 hours. The single-target distribution not only does not fit into the sample FOV based on the phased array radar at Eglin Air Force Base [16], but nearly wraps around the Earth.

D. Multi-Target Tracking of RSOs

One of the findings of [6] is that significant improvement to SSA can be made via advanced data association techniques. Traditional methods of multi-target tracking applied to SSA include multi-hypothesis trackers (MHT) [1] and Joint Probabilisitic Data Association [2]. Alternatively, more recently developed methods based on random finite sets (RFS) [12], [18] provide a framework that integrates data association with filtering, such as Probability Hypothesis Density (PHD) [19]–[21], Multi-Bernoulli [22], and Generalized Multi-Bernoulli filters [23], [24] are RFS filters that are attractive candidates for SSA applications. However, there are issues that multi-target tracking algorithms must address. These include, but are not limited to:

- Accurate modeling of target survival and detection probabilities,
- Handling spatiotemporal sparsity in measurements, and
- Modeling birth, spawning, and clutter processes.

Due to the large number of observations and tracked objects, Monte Carlo filter implementations of multi-target tracking algorithms are less attractive when compared to Gaussian mixture (GM) filter implementations. However, GM implementations are not without their own complications. To yield closed-form solutions to PDF prediction and updates, GM implementations of the PHD (GM-PHD) filter assume that the survival probability (p_S) and detection probability (p_D) are state independent. In the context of RSO tracking, the only processes that are analogous to target death include reentry, a maneuver to leave the Earth system, collision with another object, and a fragmentation event (e.g., explosion) of sufficient energy. For a catastrophic collision or fragmentation, the death of one object would also result in the birth of many smaller RSOs. Models exist to describe the distribution in number, size, and velocity change for such events (e.g., [25]), but their probability at any point in time is nearly zero.

Several factors influence the probability of detection for RSOs. Often, especially for GM-based implementations of RFS multi-target filters, p_D is assumed constant over the field of view for the sake of tractability and numeric stability. However, the actual detection probability is both a function of the sensor characteristics, the orbit environment, and the target itself. For radar sensors, the detection probability for an RSO increases as the range approaches a minimum. In terms of the orbit environment, visibility is influenced by the solar phase angle and the Earth's shadow, both of which affect p_D [26]. Finally, the instantaneous attitude and surface properties of an object influence the radar cross section and brightness, which, when coupled with a sensor's performance characteristics, yield a p_D that varies throughout a given scenario. For example, tumbling objects may appear to blink when viewed over time via an optical sensor.

The relatively large field of view for SSA sensors creates key research challenges for multi-target tracking of RSOs. For example, optical telescopes have a valid range from from just in front of the lens to infinity. Modeling birth for a nearly infinite space is not tractable, which motivates the definition of a reasonable approximation. The distribution of space objects in Fig. 1 illustrates that objects are not uniformly distributed in altitude. Optical telescope are typically used to observe objects at high altitudes (greater than 4,000 km), which includes GTOs. However, these objects pose a challenge for modeling new-target birth given their large range of orbit altitudes and a two-dimensional optical observation. Modeling birth in such a large region however, does pose significant challenges, e.g., some models fill an entire FOV with diffuse Gaussian distributions which in this case requires a computationally intractable number of GM components. This is also true for radar. Fig. 3 illustrates a radar FOV that is large enough to encapsulate a single arc of observations of a LEO object. This region requires over 7500 GM birth components, each with a radius of 100 km, to cover the FOV. Additionally, RSO tracks have states with a minimum of six dimensions which does not work well with static birth region models. While

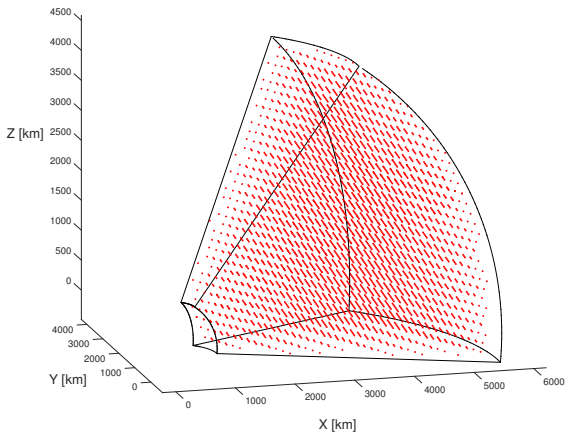

Fig. 3. Over 7500 GM birth components (centered at red dots) with radii of 100 km required to fill a FOV just large enough to capture a single arc of observations. Distances on axes represent range from sensor in the South-East-Up reference frame.

increased observation frequency allows for observing angle rates [27], this conflicts with the longer integration times that reduce clutter and increase the signal-to-noise ratio.

Modeling clutter for SSA sensors is a topic not commonly addressed in the astrodynamics literature. As mentioned previously, this may be mostly eliminated for optical sensors with larger integration times. Increased data rates allow for estimating angle rates, which produces observations with more degrees of freedom. However, clutter distribution and density models are not prominently featured in the existing RSO tracking literature. In summary, there lacks a sufficient amount of work which characterizes clutter with respect to observing RSOs.

The modeling of spawned targets is not trivial for space objects. The GM-PHD filter includes a spawning model, however, its instantaneous estimate of the number of targets is unstable [12]. The GM Cardinalized PHD (GM-CPHD) filter [28] overcomes this cardinality instability by propagating the probability distribution of the number of targets, however, classic forms of the CPHD fundamentally assume no spawning to improve tractability. Leveraging knowledge of persistent RSOs to determine the states of spawned RSOs would likely be more computationally efficient than instantiating new objects via a birth model.

III. An Astrodynamics δ-GLMB Filter

This section describes the δ-Generalized Labeled Multi-Bernoulli (δ-GLMB) and its application to tracking space objects. This first includes a brief description of the filter, commonly used models in the information fusion community, and several astrodynamics-based models employed in this paper and in previous work.

A. Filter Overview

The δ-GLMB filter yields a closed-form solution to the Bayes multi-target filter and maintains target identity through the use of a labeled RFS [23]. This section only provides an overview of the filter's properties to provide context for future discussions, and full details may be found in [23], [24].

The Bayes multi-target filter generalizes the single-target Bayes filter, but allows for simultaneous tracking of multiple targets. The δ-GLMB filter uses an approach based on a labeled Random Finite Sets (RFS) to formulate the filter. In such an approach, the multi-target state $\boldsymbol{X}_k$ and observation Y_k (at time t_k) are represented by the sets

$$\boldsymbol{X}_k = \{\boldsymbol{x}_1, \boldsymbol{x}_2, \ldots, \boldsymbol{x}_n\} \subset \mathbb{X} \times \mathbb{L} \quad (2)$$

$$Y_k = \{y_1, y_2, \ldots, y_m\} \subset \mathbb{Y} \quad (3)$$

where $\mathbb{X}$ and $\mathbb{Y}$ are the single-target state and measurement spaces, respectively, and $\mathbb{L}$ is a label space. Due to clutter and missed detections, $m = n$ is not always true. The elements of the RFS $\boldsymbol{X}$ are $\boldsymbol{x} = (x, \ell)$ where x is the estimated single-target state and $\ell = (k, j)$ denotes the j-th target newly identified at time t_k. The observation RFS Y_k is comprised of observation vectors y gathered via a single sensor scan. The δ-GLMB filter then predicts and updates the multi-target density $\boldsymbol{\pi}(\boldsymbol{X})$. The remainder of this section describes the formulation of $\boldsymbol{\pi}(\boldsymbol{X})$ that allows for deriving a closed-form solution to the Bayes multi-target filter.

The projection $\mathcal{L}(x, \ell) = \ell$ where $\mathcal{L} : \mathbb{X} \times \mathbb{L} \to \mathbb{L}$ allows for defining the set of labels $\mathcal{L}(\boldsymbol{X}) = \{\mathcal{L}(\boldsymbol{x}) : \boldsymbol{x} \in \boldsymbol{X}\}$. Since each possible target has a unique label, $|\mathcal{L}(\boldsymbol{X})| = |\boldsymbol{X}|$. To simplify notation,

$$\Delta(\boldsymbol{X}) = \delta_{|\boldsymbol{X}|}(|\mathcal{L}(\boldsymbol{X})|) \quad (4)$$

denotes a distinct label indicator and

$$\delta_A(B) \equiv \begin{cases} 1 & \text{if } B = A \\ 0 & \text{otherwise} \end{cases} \quad (5)$$

is a generalized delta function that supports sets and vectors.

The labeled multi-Bernoulli (LMB) RFS is parameterized by $\left\{\left(r^{(\ell)}, p^{(\ell)}\right)\right\}_{\ell \in \mathbb{L}}$ and the PDF of $\boldsymbol{X}$ is then

$$\boldsymbol{\pi}(\boldsymbol{X}) = \Delta(\boldsymbol{X}) w(\mathcal{L}(\boldsymbol{X})) p^{\boldsymbol{X}} \quad (6)$$

where the multi-object exponential is

$$p^{\boldsymbol{X}} \equiv \prod_{\boldsymbol{x} \in \boldsymbol{X}} p(\boldsymbol{x}) \quad (7)$$

and

$$w(L) = \prod_{i \in \mathbb{L}} \left(1 - r^{(i)}\right) \prod_{\ell \in L} \frac{1_{\mathbb{L}}(\ell) r^{(\ell)}}{1 - r^{(\ell)}} \quad (8)$$

$$p(x, \ell) = p^{(\ell)}(x), \quad (9)$$

$$1_A(B) \equiv \begin{cases} 1 & \text{if } B \subseteq A \\ 0 & \text{otherwise.} \end{cases} \quad (10)$$

The LMB density can be generalized to a mixture of multi-target exponentials, known as a generalized labeled multi-Bernoulli (GLMB)

$$\boldsymbol{\pi}(\boldsymbol{X}) = \Delta(\boldsymbol{X}) \sum_{c \in \mathbb{C}} w^{(c)}(\mathcal{L}(\boldsymbol{X})) \left[p^{(c)}\right]^{\boldsymbol{X}} \quad (11)$$

where $\mathbb{C}$ is an index set that can be used for enumerating the set of hypotheses in a multi-target tracking problem, and

$$\sum_{L\subseteq\mathbb{L}}\sum_{c\in\mathbb{C}} w^{(c)}(\mathcal{L}(\boldsymbol{X})) = 1 \quad (12)$$

$$\int p^{(c)}(x,\ell)\,dx = 1. \quad (13)$$

The δ-GLMB RFS, which is used in the filter employed here, allows for a more intuitive description of a GLMB in the context of multi-target tracking [23], [24]. For the δ-GLMB density, the index set $\mathbb{C}$ is defined over all subsets of $\mathbb{L}$ and a space Ξ representing the history of measurement associations to a given track. Hence,

$$\mathbb{C} = \mathcal{F}(\mathbb{L})\times\Xi \quad (14)$$

$$w^{(c)}(L) = w^{(I,\xi)}\delta_I(L) \quad (15)$$

$$p^{(c)} = p^{(I,\xi)} = p^{(\xi)} \quad (16)$$

where $c=(I,\xi)$, $\xi\in\Xi$, $I\subset\mathbb{L}$, and the function $\mathcal{F}(\mathbb{L})$ represents the collection of all finite subsets of $\mathbb{L}$. Then, the δ-GLMB density is given by

$$\boldsymbol{\pi}(\boldsymbol{X}) = \Delta(\boldsymbol{X}) \sum_{(I,\xi)\in\mathcal{F}(\mathbb{L})\times\Xi} w^{(I,\xi)}\delta_I(\mathcal{L}(\boldsymbol{X}))\left[p^{(\xi)}\right]^{\boldsymbol{X}}. \quad (17)$$

The δ-GLMB is distinguished from the GLMB by the construction of the space $\mathbb{C}$ imposed in its formulation. In the following sections, a hypothesis refers to a single pair (I,ξ) that describes a set of targets by the label set I and measurement association history ξ. The weight $w^{(I,\xi)}$ then describes the probability of hypothesis (I,ξ).

Given this formulation of the δ-GLMB PDF, [23] presents a closed-form solution to the Bayes multi-target filter. Like all sequential filters, this includes both a prediction to a time of interest followed by a measurement update. The prediction can account for target survival, death, and the appearance of new targets. For new-target birth, the δ-GLMB filter assumes a labeled multi-Bernoulli model that is parameterized by $\left\{\left(r_B^{(i)},p_B^{(i)}\right)\right\}_{i=1}^{N_B}$ where $r_B^{(i)}$ is the probability that the i-th target exists, and $p_B^{(i)}$ is the single-target PDF. Details on the birth and single-target propagation models employed here may be found in the following sections. The measurement update provides a framework to include probability of detection and a clutter model. The full prediction and measurement update equations may be found in [24].

B. Astrodynamics-Based Models

This section describes models commonly used for astrodynamics with analogues in multi-target filtering. This includes both models for new-target birth and more computationally efficient non-Gaussian single-target PDF propagation.

As discussed previously, a prior Gaussian single-target PDF for a space object will not necessarily remain Gaussian under prediction. Traditionally, the tracking of space objects uses a batch least-squares filter with Gaussian assumptions [6]. Recent research instead proposes non-Gaussian methods for use in nonlinear, single-target filters. This includes both Gaussian mixtures [29] and particle filters [30]. In the case of Gaussian mixtures, entropy-based methods of component splitting [29] and alternative representations of the state vector [17] yield a reduction in computation costs. The results presented later in this paper use the entropy-based method for splitting components as needed.

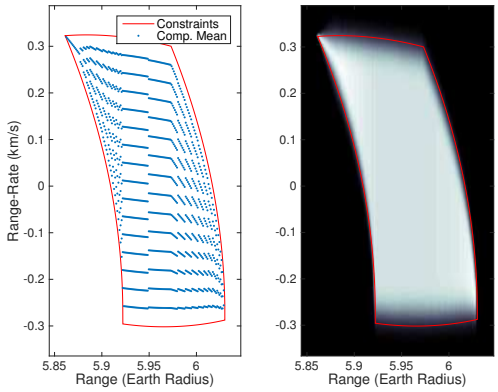

Fig. 4. Illustration of admissible region for new-target birth

In the context of astrodynamics, target birth is referred to as initial orbit determination (IOD). Given the underdetermined state estimation problem when given a single observation, IOD is typically performed via observation-to-observation association. Methods vary based on the observations available, e.g., Gauss's technique may be used when provided angles-only observations. However, observation-to-observation association is sometimes difficult due to the potentially large measurement gaps. A detailed description of the classical methods for IOD may be found in [16] and such methods have found use in multiple-hypothesis trackers [1]. For an RFS-based filter, the use of observations at multiple epochs to aid in modeling new-target birth requires the use of smoothing [31]. At present there are two multiobject smoothing solutions: forward-backward (FB) smoothing [31]; and batch smoothing [32]. In [31], Gaussian mixture forward-backward smoothing solutions for single-target, Bernoulli and PHD filters are given. The batch solution [32] is quite generic, and needs to be adapted to SSA for better efficiency. It is also important to develop efficient FB smoothing algorithms for label RFS filters. Alternatively, RFS-based filters may employ a diffuse GM model for new-target birth or a uniform distribution in the measurement space [33]. As described later, such models require astrodynamics-based augmentations to allow for their use.

More recently developed techniques for IOD instead consider a combination of high-dimensional observations, e.g., angles with angle rates, with physics-based constraints. For example, when observing orbital debris, a maximum semimajor axis may be considered. For the case of the observation vector $\boldsymbol{z}=\begin{bmatrix}\alpha & \delta & \dot{\alpha} & \dot{\delta}\end{bmatrix}$ where α and β are angles, then there is no information on the range or range-rate for the target. Constraints may then be added to reduce the space of possible

solutions, which is referred to as the admissible region (AR). Such methods have been applied for orbital debris [34], [35] and represent a subject of active research in astrodynamics. One possible method of leveraging this AR is to consider all points within the constraints as equally probable, which yields a uniform distribution over the AR. One may then sample the distribution to create virtual objects [36] (with potential use in a particle filter) or approximate the distribution using a Gaussian mixture [34]. Fig. 4 illustrates such a GM-based approximation of the admissible region with constrains defined by semimajor axis and eccentricity. This method is used to generate $p_B^{(i)}$ in the δ-GLMB birth model with the existence probability determined using the method proposed in [37]. This GM model shares some similarities to the partially-uniform birth model in [33], but the mixture in range and range-rate directions is not independent of the angle and angle-rate measurements.

IV. Simulations and Results

This section describes the performance of the δ-GLMB filter for different astrodynamics and non-astrodynamics based models. All accuracy comparisons use the optimal sub-pattern assignment (OSPA) [38] metric to describe accuracy. These use $c = 100$ km, $p = 2$, and ignore the cardinality penalty function. For all cases, $p_S = 0.99$.

The orbits simulated in the following sections all use the CU-TurboProp orbit propagation package [39]. This includes orbit propagation software written in C/C++ with a MATLAB or Python interface. This work used the Dormand-Prince 8(7) embedded Runge-Kutta integrator with an relative tolerance of 10^{-12}. Force models include the GGM03C gravity perturbation model of degree 20 (for low-Earth orbit) or 8 (for geosynchronous orbit). Third-body gravity forces include those generated by the Sun and the Moon using the DE430 ephemeris. Solar radiation pressure (SRP) is included with a reflectivity coefficient of 1.5. Atmospheric drag is included at low altitudes with a drag coefficient of 2.15 and an exponential density model. Both the SRP and drag use a constant area-to-mass ratio of 0.01 m^2/kg, which corresponds to a spherical body. For a description of these force models, see [39] and the references therein. Studies with a larger array of shapes and attitude profiles should be considered in future work.

A. Computation Considerations

To illustrate the relative performance of UKF-, GMM-, and SMC-based solutions to tracking space objects with the δ-GLMB filter, the scenario in this section considers two LEO targets. To simplify the test and better isolate the effects of single-target PDF propagation on the computation time, this case assumes zero false alarms, i.e., no clutter measurements. A single ground station (located in Maui, HI) gathers range and range-rate (analogous to Doppler) observations of the targets with an approximately 34 hour gap between data arcs. Over this duration, the spacecraft completes approximately 20 orbits and has a highly non-Gaussian single-target PDF at the start of the second arc. (Note that this is not the same orbit

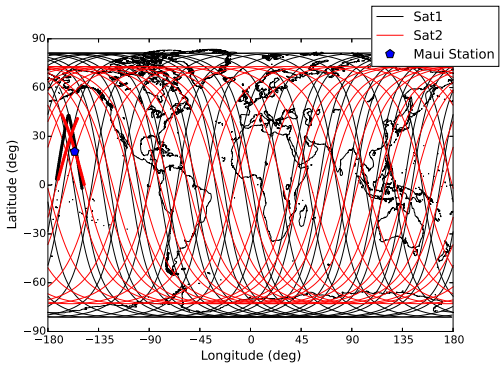

Fig. 5. Groundtracks and measurement arcs (thicker lines) for the two LEO spacecraft

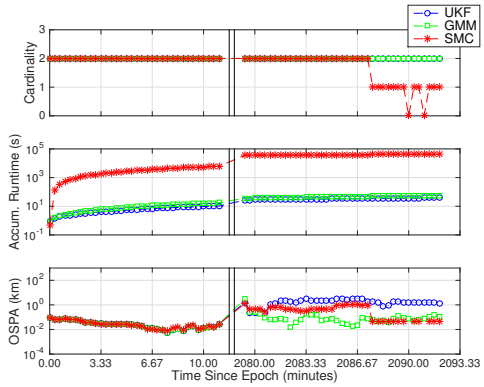

Fig. 6. Performance of the UKF-, GMM, and SMC-based implementations of the δ-GLMB filter for the LEO case. The double black lines denote the ~34-hour data gap.

depicted in Fig. 2.) The range and range-rate measurement errors have zero mean and standard deviations of 10 m and 75 cm/s, respectively. Fig 5 illustrates the ground tracks for these orbits along with the measurement arcs. The observed period of the orbit represents a small portion of the total trajectory and illustrates the spatiotemporal data limitations in such a scenario.

Fig. 6 illustrates the performance of a UKF, GMM, and SMC-based implementation of the δ-GLMB filter. The GMM case uses the entropy-based splitting of Gaussian components during the prediction step. The SMC results used 100,000 particles per target. Both the UKF- and GMM-based implementations of the filter maintain custody of the two targets at all measurement times. The SMC-based filter loses custody of one target during the second arc due to an insufficient number of particles. The SMC filter also required hours to process the data while the GMM version only requires minutes. Finally, the GMM filter provides accuracy for two targets comparable to the single-target SMC result (for one target).

B. Modeling Birth

This section describes the performance of a fixed GM model and the AR-based birth model for a GEO scenario. In this

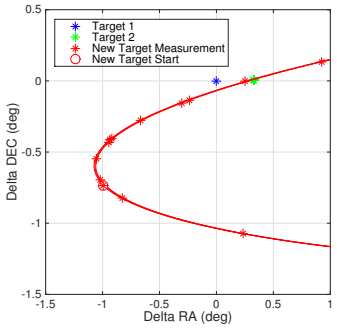

Fig. 7. Motion of targets 2 and 3 relative to target 1 in the measurement space.

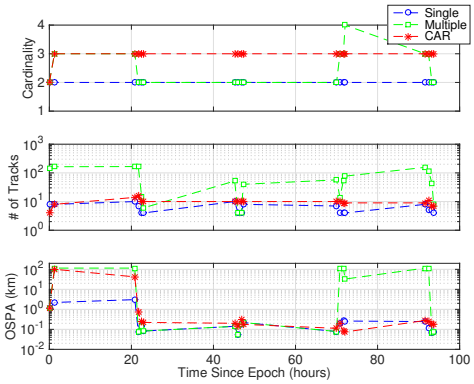

Fig. 8. Filter performance for sparse measurements and the different birth models

case, two initially known targets are observed by an optical sensor, see Fig. 7. Observations are 4-D angle and angle rates with error standard deviations of 0.4 arcsec and 0.07 arcsec/s, respectively. No clutter is included in this case and $p_D = 0.99$.

Fig. 8 illustrates the performance of the various birth models for this scenario. The case dubbed *Single* refers to a fixed GM-based birth model were all components are treated as a mixture for a single possible new target. While this improves tractability by reducing the number of birth hypotheses, it limits the filter to only one new target per scan. Alternatively, the *Multiple* case considers each GM component as a possible new target and increases the number of birth hypotheses in the filter. Finally, the *CAR* case uses the measurement-based birth model and the constrained admissible region to model new-target generation. These results demonstrate that the CAR case yields the best accuracy at a slight reduction in the number of tracks maintained in the δ-GLMB filter. The number of tracks indicates the number of estimated states propagated and updated in the filter and provides a measure of computation time. The single-target birth model case is unable to maintain knowledge of any birth targets to yield a positive identification. Specifically, any hypotheses that contain a new target (at any time) are deemed unlikely and eventually pruned. The multiple-target birth model identifies that a new target exists, but is unable to maintain custody of the object with the

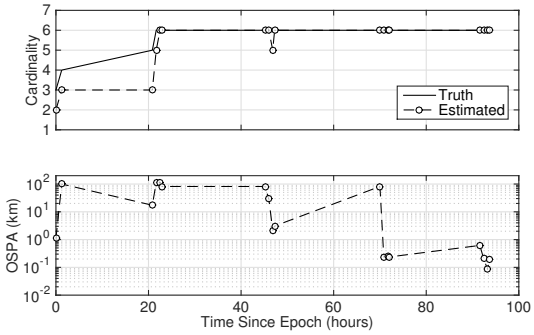

Fig. 9. Filter performance for the case with six targets

long data gaps. Fluctuations in the number of targets for the multiple-birth case result from the filter attempting to reacquire the target with subsequent measurements. Although not illustrated in the figure, the label for the new target in the Multiple case changes over time indicating a failure to maintain custody of the target. The CAR-based method identifies the new target, maintains the correct labels, and converges on a solution after the approximately 90-hour simulation duration.

C. Increased Number of Targets

This scenario considers a larger number of unknown targets. Whereas the previous case demonstrates the inability of a simple fixed GM-based birth model to maintain custody of a new target when given insufficient observation density, this case extends the CAR-based method to identifying multiple new targets using the same observation sparsity. In addition to the three targets in the previous scenario, three new targets are introduced. These previously unknown targets appear at the second, third, and fourth observation scans and have orbits that are random perturbations in semimajor axis and inclination of target 1. In addition to the increased number of targets, this case includes clutter with a mean rate of one return per scan and a reduced detection probability ($p_D = 0.9$).

Fig. 9 provides the estimated number of tracks and the OSPA accuracy of the δ-GLMB filter for this six-target case. A delay exists between a target first appearing and the filter confirming its existence, but the filter maintains custody of the targets at subsequent points in time. The temporary cardinality decrease at approximately 45 hours results from consecutive missed detections for the third target. The OSPA distance indicates that the solution converges to state-estimation errors on the order of hundreds of meters, which is consistent with the observation errors for this scenario. Labels for the new targets at the final time correspond to the correct time of birth.

V. Conclusions

This paper discussed the difficulties of multi-target tracking of RSOs. This included an overview of SSA requirements and the potential uses of an estimated multi-target state. The discussion included an introduction to issues related to modeling the dynamics of space objects and the sensors currently employed for generated measurements. Several of the issues

were then illustrated in the context of the δ-GLMB RFS-based multi-target filter. This included the difficulties in modeling the non-Gaussian single-target state PDF and the limitations of using a diffuse Gaussian model for the prior state of new targets. A δ-GLMB filter that leverages a birth model based on astrodynamics principles allows for tracking both known and previously unknown objects with sparse observations.

ACKNOWLEDGMENTS

The authors thank Ben Bradley for providing the two-line element software used to generate Fig. 1. The authors also thank Marc Balducci for generating the propagated samples used in Fig. 2 to illustrate the space object PDF.

REFERENCES

[1] N. Singh, J. T. Horwood, J. M. Aristoff, A. B. Poore, C. Sheaff, and M. K. Jah, "Multiple hypothesis tracking (MHT) for space surveillance: Results and simulation studies," in *Proceedings of the 2013 Advanced Maui Optical and Space Surveillance Technologies Conference*, (Wailea, Maui, Hawaii), September 2013.

[2] J. Stauch, M. Jah, J. Baldwin, T. Kelecy, and K. A. Hill, "Mutual application of joint probabilistic data association, filtering, and smoothing techniques for robust multiple space object tracking (invited)," in *AIAA/AAS Astrodynamics Specialist Conference*, American Institute of Aeronautics and Astronautics, 2015/02/26 2014.

[3] I. I. Hussein, K. J. DeMars, C. Früh, M. K. Jah, and R. S. Erwin, "An AEGIS-FISST algorithm for multiple object tracking in space situational awareness," in *AIAA/AAS Astrodynamics Specialist Conference*, (Minneapolis, Minnesota), August 13-16 2012.

[4] B. A. Jones, S. Gehly, and P. Axelrad, "Measurement-based birth model for a space object cardinalized probability hypothesis density filter," in *AIAA/AAS Astrodynamics Specialist Conference*, (AIAA 2014-4311, San Diego, California), August 4-7 2014.

[5] B. A. Jones and B.-N. Vo, "A labeled multi-Bernoulli filter for space object tracking," in *2014 AAS/AIAA Spaceflight Mechanics Meeting*, (AAS 15-413, Williamsburg, VA), January 11-15 2014.

[6] Committee for the Assessment of the U.S. Air Force's Astrodynamic Standards; Aeronautics and Space Engineering Board; Division on Engineering and Physical Sciences; National Research Council, *Continuing Kepler's Quest: Assessing Air Force Space Command's Astrodynamics Standards*. The National Academies Press, 2012.

[7] J. Woodburn, V. Coppola, and F. Stoner, "A description of filters for minimizing the time required for orbital conjunction computations," in *AAS/AIAA Astrodynamics Specialist Conference*, (Pittsburgh, PA), August 9-13 2009.

[8] M. D. Lichter and S. Dubowsky, "State, shape, and parameter estimation of space objects from range images," in *Robotics and Automation, 2004. Proceedings. ICRA '04. 2004 IEEE International Conference on*, vol. 3, pp. 2974–2979 Vol.3, April 2004.

[9] R. Linares, M. K. Jah, J. L. Crassidis, F. A. Leve, and T. Kelecy, "Astrometric and photometric data fusion for inactive space object mass and area estimation," *Acta Astronaut.*, vol. 99, pp. 1 – 15, 2014.

[10] T. Schildknecht, R. Musci, M. Ploner, G. Beutler, W. Flury, J. Kuusela, J. de Leon Cruz, and L. de Fatima Dominguez Palmero, "Optical observations of space debris in GEO and in highly-eccentric orbits," *Adv. Space Res.*, vol. 34, no. 5, pp. 901–911, 2004.

[11] D. P. Lubey and D. J. Scheeres, "An optimal control based estimator for maneuver and natural dynamics reconstruction," in *Proceedings of the 2013 Advanced Maui Optical and Space Surveillance Technologies Conference*, (Wailea, Maui, Hawaii), September 2013.

[12] R. P. S. Mahler, *Advances in Statistical Multisource-Multitarget Information Fusion*. Boston, Massachusetts: Artech House, 2014.

[13] J. L. Junkins, M. R. Akella, and K. T. Alfriend, "Non-Gaussian error propagation in orbital mechanics," *J. Astronaut. Sci.*, vol. 44, pp. 541–563, October - December 1996.

[14] H. Klinkrad, *Space Debris: Models and Risk Analysis*. Chichester, England: Springer Praxis Books, 2006.

[15] B. D. Tapley, B. E. Schutz, and G. H. Born, *Statistical Orbit Determination*. Burlington, MA: Elsevier Academic Press, first ed., 2004.

[16] D. A. Vallado and W. D. McClain, *Fundamentals of Astrodynamics and Applications*. Hawthorne, CA and New York, NY: Microcosm Press and Springer, third ed., 2007.

[17] J. T. Horwood, N. D. Aragon, and A. B. Poore, "Gaussian sum filters for space surveillance: Theory and simulations," *J. Guid. Control. Dyn.*, vol. 34, pp. 1839–1851, November - December 2011.

[18] R. P. S. Mahler, *Statistical Multisource-Multitarget Information Fusion*. Boston, Massachusetts: Artech House, 2007.

[19] R. P. S. Mahler, "Multitarget Bayes filtering via first-order multitarget moments," *Aerosp. Electron. Syst. IEEE Transactions on*, vol. 39, pp. 1152–1178, Oct 2003.

[20] B.-N. Vo, S. Singh, and A. Doucet, "Sequential Monte Carlo methods for multitarget filtering with random finite sets," *Aerosp. Electron. Syst. IEEE Transactions on*, vol. 41, pp. 1224–1245, Oct 2005.

[21] B.-N. Vo and W.-K. Ma, "The Gaussian mixture probability hypothesis density filter," *IEEE Transactions on Signal Process.*, vol. 54, pp. 4091–4104, November 2006.

[22] B.-T. Vo, B.-N. Vo, and A. Cantoni, "The cardinality balanced multi-target multi-Bernoulli filter and its implementations," *IEEE Transactions on Signal Process.*, vol. 57, pp. 409–423, February 2009.

[23] B.-T. Vo and B.-N. Vo, "Labeled random finite sets and multi-object conjugate priors," *IEEE Transactions on Signal Process.*, vol. 61, pp. 3460–3475, July 2013.

[24] B.-N. Vo, B.-T. Vo, and D. Phung, "Labeled random finite sets and the Bayes multi-target tracking filter," *IEEE Transactions on Signal Process.*, vol. 62, pp. 6554–6567, December 2014.

[25] N. L. Johnson, P. H. Krisko, J.-C. Liou, and P. D. Anz-Meador, "NASA's new breakup model of EVOLVE 4.0," *Adv. Space Res.*, vol. 28, no. 9, pp. 1377–1384, 2001.

[26] C. Früh and M. K. Jah, "Detection probability of earth orbiting objects using optical sensors," in *AAS/AIAA Astrodynamics Specialist Conference*, (Paper AAS 13-701, Hilton Head, SC), August 11-15 2013.

[27] J. M. Maruskin, D. J. Scheeres, and K. T. Alfriend, "Correlation of optical observations of objects in Earth orbit," *J. Guid. Control. Dyn.*, vol. 32, pp. 194–209, January-February 2009.

[28] B.-T. Vo, B.-N. Vo, and A. Cantoni, "Analytic implementations of the cardinalized probability hypothesis density filter," *IEEE Transactions on Signal Process.*, vol. 55, pp. 3553–3567, July 2007.

[29] K. J. DeMars, R. H. Bishop, and M. K. Jah, "Entropy-based approach for uncertainty propagation of nonlinear dynamical systems," *J. Guid. Control. Dyn.*, vol. 36, pp. 1047–1057, July-August 2013.

[30] A. Mashiku, J. L. Garrison, and J. R. Carpenter, "Statistical orbit determination using the particle filter for incorporating non-Gaussian uncertainties," in *AIAA/AAS Astrodynamics Specialist Conference*, (Minneapolis, Minnesota), August 13-16 2012.

[31] B.-N. Vo, B.-T. Vo, and R. P. S. Mahler, "Closed-form solutions to forward-backward smoothing," *IEEE Transactions on Signal Process.*, vol. 60, pp. 2–17, January 2012.

[32] T. Vu, B.-N. Vo, and R. Evans, "A particle marginal Metropolis-Hastings multi-target tracker," *IEEE Transactions on Signal Process.*, vol. 62, pp. 3953–3964, August 2014.

[33] M. Beard, B.-T. Vo., B.-N. Vo, and S. Arulampalam, "A partially uniform target birth model for Gaussian mixture PHD/CPHD filtering," *Aerosp. Electron. Syst. IEEE Transactions on*, vol. 49, pp. 2835–2844, October 2013.

[34] K. J. DeMars and M. K. Jah, "Probabilistic initial orbit determination using Gaussian mixture models," *J. Guid. Control. Dyn.*, vol. 36, pp. 1324–1335, September - October 2013.

[35] K. Fujimoto, D. J. Scheeres, J. Herzog, and T. Schildknecht, "Association of optical tracklets from a geosynchronous belt survey via the direct Bayesian admissible region approach," *Adv. Space Res.*, vol. 53, no. 2, pp. 295–308, 2014.

[36] G. Tommei, A. Milani, and A. Rossi, "Orbit determination of space debris: admissible regions," *Celest. Mech. Dyn. Astron.*, vol. 97, no. 4, pp. 289–304, 2007.

[37] S. Reuter, B.-T. Vo, B.-N. Vo, and K. Dietmayer, "The labeled multi-Bernoulli filter," *IEEE Transactions on Signal Process.*, vol. 62, pp. 3246–3260, June 2014.

[38] D. Schuhmacher, B.-T. Vo, and B.-N. Vo, "A consistent metric for performance evaluation of multi-object filters," *IEEE Transactions on Signal Process.*, vol. 56, pp. 3447–3457, August 2008.

[39] K. Hill and B. A. Jones, *TurboProp Version 4.0*. Colorado Center for Astrodynamics Research, May 2009.